Journal of Photochemistry and Photobiology A: Chemistry 216 (2010) 238–243

Contents lists available at ScienceDirect

Journal of Photochemistry and Photobiology A: Chemistry

journal homepage: www.elsevier.com/locate/jphotochem

In situ EPR studies of electron trapping in a nanocrystalline rutile

I. Ross Macdonald [a], Russell F. Howe [a,*], Xinyuan Zhang [b], Wuzong Zhou [b]

[a] Chemistry Department, University of Aberdeen, Aberdeen AB24 3UE, Scotland, United Kingdom
[b] School of Chemistry, University of St Andrews, St Andrews KY16 9ST, Scotland, United Kingdom

ARTICLE INFO

Article history:
Available online 30 July 2010

Keywords:
Rutile
EPR
Trapped electrons
Trap sites

ABSTRACT

This paper describes an in situ EPR study of electron trapping in a nanocrystalline rutile material. Irradiation at 4 K with broad-band UV–Vis light gives weak signals of trapped electrons. When irradiation is stopped, intense Ti^{3+} EPR signals appear, which can be removed again by resuming the irradiation. It is proposed that under irradiation there is a dynamic equilibrium established between creation of conduction band electrons, trapping of electrons, and excitation from trap sites back into the conduction band. When irradiation is stopped, conduction band electrons are trapped and remain so in the dark. Some initial results on the temperature and wavelength dependence of these processes are presented.

1. Introduction

Oxide semiconductors feature widely in attempts to design new materials for solar energy conversion. Crucial to this ambition, as well as to conventional photocatalysis, is the efficient separation of charge carriers produced by band-gap irradiation of the semiconductor. The processes of hole and electron trapping and recombination are however poorly understood, despite the importance of these events to applications of semiconductor photocatalysis.

EPR spectroscopy, which observes and identifies 1-electron species with high sensitivity, has been applied by several groups to study hole and electron trapping in titanium dioxide. Howe and Graetzel first showed that UV irradiation of anatase in vacuo at low temperatures produces EPR signals assigned to trapped holes (O^- radical anions) and trapped electrons (Ti^{3+}), which recombined slowly in the dark at 4 K, and more rapidly at higher temperatures [1]. The dynamics of hole and electron trapping in nanocrystalline anatase were subsequently investigated in detail by Berger et al. [2,3] who showed that trapping of holes and electrons occurs on a time scale of seconds to minutes at 90 K during in situ irradiation. The spin concentrations of trapped holes exceeded that of the trapped electrons, and the discrepancy was attributed to the formation of delocalised conduction band electrons which are EPR silent. Support for this explanation came from the observation of a broad infrared absorption due to conduction band electrons when anatase was irradiated in vacuo. Oxygen was shown to scavenge both conduction band and trapped electrons, producing an enhanced intensity for the trapped hole (O^-) signal as well as the superoxide ion O_2^-, the product of electron scavenging.

The trapping of holes and electrons in anatase has also been shown by Berger et al. [4] to depend on the intensity of UV irradiation. At higher UV irradiance, a direct non-radiative recombination pathway becomes important, and sample heating by as much as 25 K is observed.

Charge trapping in rutile has received less attention. EPR spectroscopy has been used by Hurum et al. to develop an explanation for the enhanced photocatalytic activity of mixed phase anatase plus rutile catalysts such as Degussa P25 [5,6]. In this model, electrons produced in the conduction band of rutile (which has a smaller band-gap than anatase) are transferred to trap sites within the band-gap of anatase, and the interface between the two phases plays a crucial role in the enhanced photocatalytic performance. Komaguchi et al. [7], on the other hand, have shown EPR evidence for photo-induced electron transfer from anatase to rutile. In pure anatase, they found that electrons trapped as Ti^{3+} could be excited back into the conduction band by excitation with sub band-gap radiation; in the presence of rutile, these anatase conduction band electrons were then trapped at rutile surface sites.

In the case of pure rutile, Kumar et al. reported briefly that trapped electron and trapped hole signals could be seen in UV irradiated rutile at low temperatures similar to those seen for anatase [8]. More recently Yang et al. have observed photo-induced sites in single crystals of rutile irradiated with 442 nm laser light. They identified trapped electron sites as singly ionised and neutral oxygen vacancies, with the unpaired electron spins localised on single

* Corresponding author.
E-mail address: r.howe@abdn.ac.uk (R.F. Howe).

1010-6030/$ – see front matter © 2010 Elsevier B.V. All rights reserved.
doi:10.1016/j.jphotochem.2010.07.023

or pairs of adjacent Ti^{3+} ions, respectively. Hole trapping was considered to occur at impurity Fe^{3+} and Cr^{3+} dopant ions, and the ability of sub-band-gap radiation to generate trapped electrons was attributed to photo-excitation of electrons from impurity dopant levels within the band-gap rather than from the conduction band [9]. Komaguchi et al. have recently described an EPR study of pre-reduced rutile on which superoxide ions are formed spontaneously when oxygen is admitted. Subsequent visible light illumination caused a growth of both superoxide and Ti^{3+} signals, which was attributed to a visible light driven transfer of electrons from peroxide ions formed on the reduced rutile surface [10]. Scotti et al. irradiated a sol–gel rutile sample in a helium atmosphere at 10 K, and obtained a spectrum dominated by trapped holes (O^-), with a very weak contribution from a trapped electron (Ti^{3+}) signal [11].

Given the paucity of data on electron and hole trapping processes in polycrystalline rutile, not withstanding the importance of rutile alone or in contact with anatase as a photocatalyst, and the availability of single crystal data for rutile, we have begun a detailed investigation of species formed on UV or visible light irradiation of a commercial nanocrystalline rutile material using in situ EPR spectroscopy, and we report here some initial results from that study.

2. Materials and methods

The rutile sample used for these experiments was an experimental nanoparticulate rutile supplied by CRODA International PLC. The X-ray powder diffraction pattern was obtained using a Bruker D8 diffractometer, operating with Cu K X-rays. A Varian Cary 50 Scan UV–Vis spectrophotometer, equipped with a diffuse reflectance accessory, was used acquire the absorption spectrum of the rutile. The band-gap was determined by plotting the product of the square of the Kubelka–Munk function with photon energy, against photon energy, following Ref. [12].

Transmission electron micrographs (TEM) were obtained with a JEOL JEM2011 electron microscope operated at 200 kV and equipped with a Gatan 794 CCD camera.

For EPR experiments, rutile samples (typically ~10 mg) were placed in a quartz high vacuum EPR vacuum cell and evacuated overnight to remove loosely bound water and atmospheric gases from the cell. Precautions were taken to exclude all hydrocarbon contamination: the EPR cells and the vacuum line contained no greased joints or stopcocks, and the vaccum line achieved a base pressure of below 10^{-6} mbar with a turbomolecular pump backed by an oil-free scroll pump. EPR cells were then placed in the cavity of a JEOL JES-FA200 EPR spectrometer operating with an X-band microwave source at 9.1 GHz. The magnetic field was calibrated with a Mn^{2+} marker. An Oxford Instruments ESR 900 cryostat used liquid helium or liquid nitrogen to achieve the desired temperatures. Temperatures were controlled with an ITC 503S Intelligent Temperature Controller. Sample temperatures were measured with a Lakeshore CX1050 Cernox sensor located 2 mm below the sample. The samples were irradiated in situ using a 450 W Lot Hg(Xe) light source, which was focused into the sample cavity with a lense mounted on the front of the cavity. The light source was equipped with a Pyrex glass filter (cut-off at ~320 nm) and a water filter (cut-off ~900 nm) to remove the 'hard-UV' and infrared wavelengths respectively. Visible light filters, supplied by Andover Corporation were used to irradiate the samples with different wavelengths of light. The filters allowed a narrow range (ca. 60 nm bandwidth) of wavelengths to reach the sample.

3. Results and discussion

3.1. Characterisation of rutile sample

Fig. 1 shows a low magnification TEM image of the nanocrystalline rutile. The material was found to comprise a mixture of needle-shaped particles and smaller crystals with approximately cubic morphology. The needle-shaped particles varied in length between 16 and 80 nm (average 32–36 nm) and in width between 6 and 18 nm (average 10–14 nm), while the smaller crystals were between 5 and 10 nm across. High-resolution TEM (HRTEM) images confirmed that both the needles and the cubes were crystalline rutile with a tetragonal unit cell (a = 0.458 nm, c = 0.295 nm). Fig. 2(a) shows for example an HRTEM image of part of a needle-like crystal. The marked d-spacings of 0.218 nm are indexed as (1 1 1) planes of rutile. Some needle-shaped particles are single crystalline, but the majority are polycrystalline, and contain many voids. A similar conclusion is reached from the HRTEM image of a cube-like crystal in Fig. 2(b). The image shows a square contrast pattern with d-spacings of 0.333 nm, indexed to (1 1 0) and (1 $\bar{1}$ 0) planes of rutile. Some voids (indicated by arrows) are also present in the cubic crystals, as well as defects associated with lattice distortions and atomic dislocations.

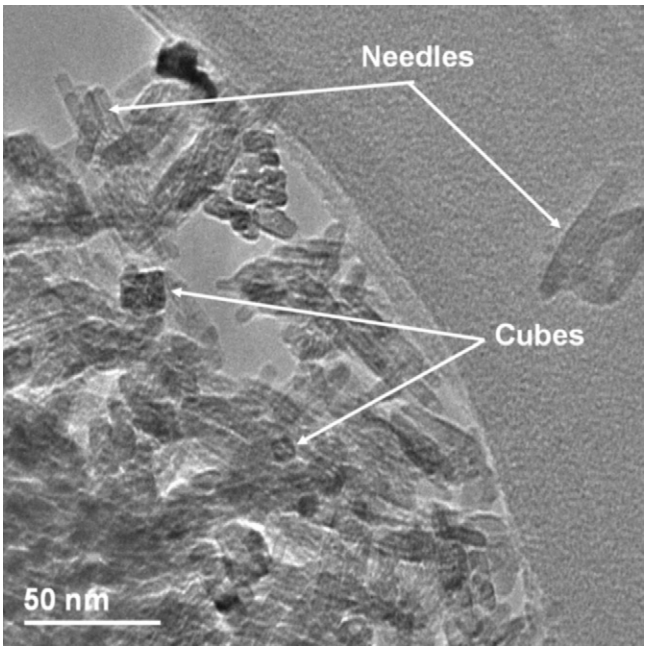

Fig. 1. Low magnification TEM image of nanorutile sample.

The X-ray powder diffraction pattern of the rutile sample (Fig. 3) confirmed that rutile is the only crystalline phase present on a macroscopic scale. The lines are relatively broad, consistent with the particle sizes seen in the electron micrographs. (The variations in crystal morphology made estimates of particle size from the powder diffraction of little value).

Fig. 4 shows the UV–Vis diffuse reflectance spectrum of the rutile. The absorption edge is relatively sharp, at about 415 nm (point of steepest slope). The absence of significant tailing on the absorption edge is consistent with the high crystallinity revealed in HRTEM images. As shown in the inset to Fig. 4, the band-gap determined by the conventional method is 3.15 eV, which can be compared with a literature value for crystalline rutile of 3.02 eV [13].

3.2. Photoreactivity of rutile

Fig. 5 shows results of an experiment in which rutile outgassed at room temperature was irradiated sequentially at 4 K with narrow band radiation of decreasing wavelength, beginning at 700 nm. All spectra show a signal at ~g = 2 which is due to a defect in the quartz tubing of the cryostat (and is present before irradiation). No new

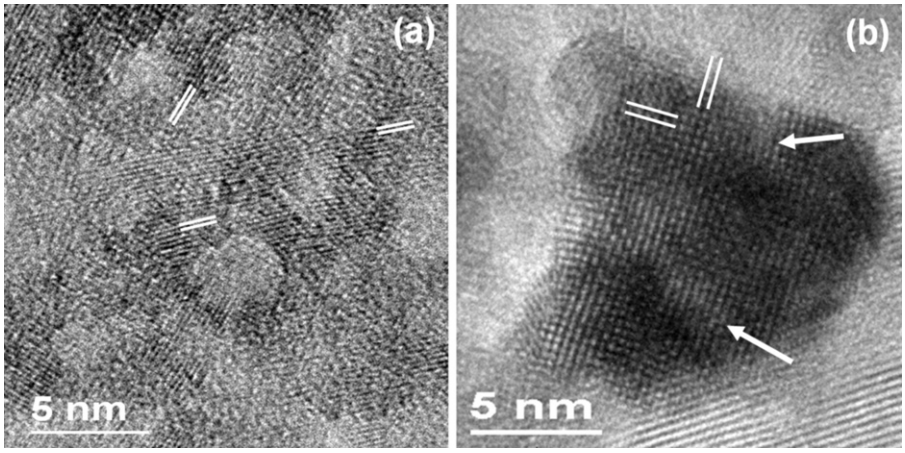

Fig. 2. HRTEM images of portion of needle-like crystal (a) and (b) cube-like crystal.

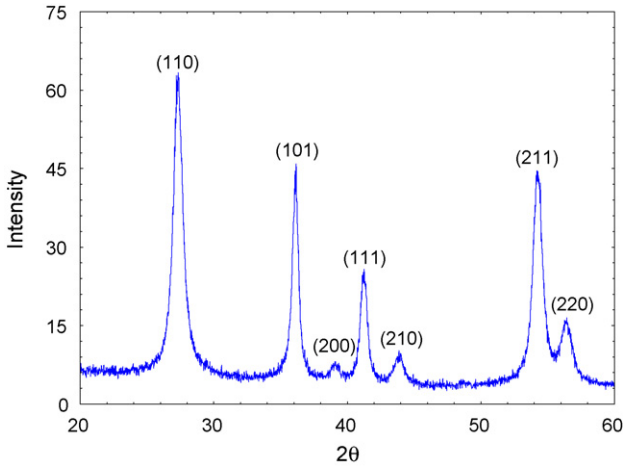

Fig. 3. X-ray powder diffraction pattern of nanocrystalline rutile sample.

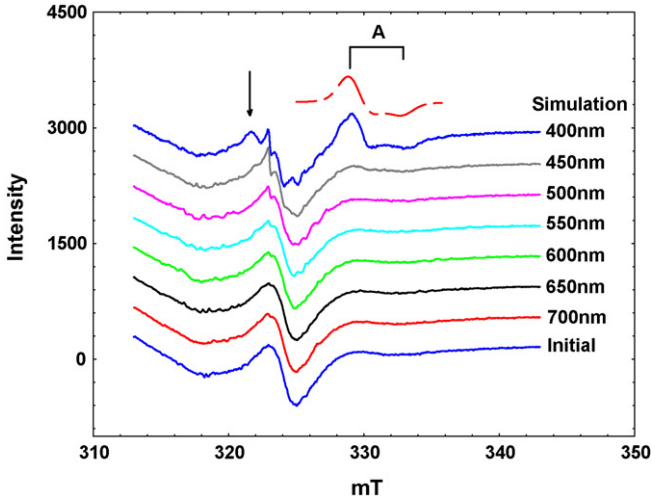

Fig. 5. EPR spectra recorded at 4 K on irradiation of rutile sample outgassed at room temperature with light of selected wavelengths. The signal at 324 mT present in the initial spectrum is due to a defect in the cryostat quartz tubing. The arrow indicates the $g_{\perp}$ feature of trapped holes (O^-). The dashed trace is a simulation of the Ti^{3+} signal A using the parameters given in the text.

signals appeared until the irradiating wavelength reached 450 nm (i.e. overlapping with the onset of the absorption edge). At this point very weak signals were superimposed on the quartz background which appeared to be due to methyl radicals (a 1:3:3:1 quartet with a spacing of 2.3 mT), and a weak feature appeared at higher field ($\sim g = 1.96$) in the region expected for Ti^{3+}. On irradiation at 400 nm, the Ti^{3+} signal became clearly developed. The *g*-tensor components for this signal were determined by matching the observed spectrum to a calculated powder pattern. The signal (identified here as Ti^{3+} species A) has $g_{\perp} = 1.971$ and $g_{\parallel} = 1.950$. At lower field, the spectrum obtained during irradiation at 400 nm shows in addition to the methyl radical signal clear evidence of the $g_{\perp}$ component($\sim$2.018) of the trapped hole (O^-) species reported previously in irradiated anatase [1–4]. When radiation was stopped, all of the new signals decayed slowly in intensity over a period of many minutes in the dark at 4 K.

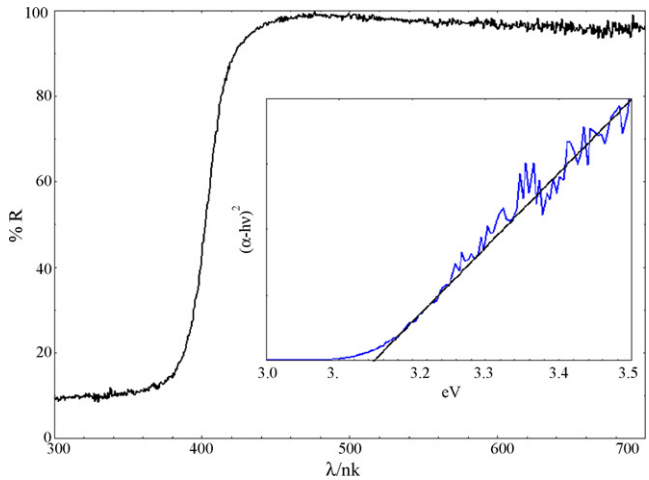

Fig. 4. UV–Vis diffuse reflectance spectrum of nanocrystalline rutile sample.

The appearance of trapped electrons (Ti^{3+}) and trapped holes (O^-) on irradiation with light of wavelength overlapping the absorption edge is completely consistent with what happens with anatase [1–4]. We have found that signals due to methyl radicals are frequently formed when anatase and rutile samples contaminated with organic impurities are irradiated in situ; this is attributed to the facile attack of photo-generated holes on adsorbed molecules containing methyl groups, cleaving C–C or C–O bonds. In the present experiments, notwithstanding the efforts taken to avoid hydrocarbon contamination, some trace amounts are evidently still present.

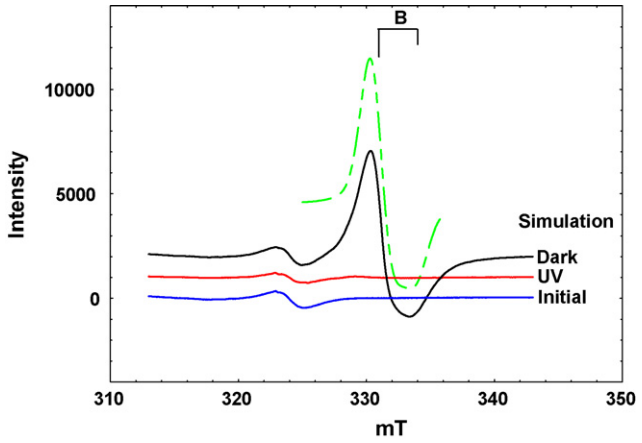

Fig. 6. EPR spectra obtained on irradiation of rutile sample outgassed at room temperature with 450 mW broad-band (320–900 nm) light. The dashed trace shows a simulation of the Ti^{3+} signal B described in the text.

Very different results were obtained when rutile samples outgassed at room temperature were irradiated with broad-band (320–900 nm) light at 4 K. In this case, under steady-state irradiation, the weak signals due to trapped electrons seen on 400 nm irradiation were again detected, but no trapped holes were seen. The quartz defect signal was attenuated by a factor of ~2, consistent with a temperature rise of ca. 4 K during in situ irradiation (Fig. 6), When irradiation was stopped, an intense new signal immediately appeared due to trapped electrons. This signal, assigned to Ti^{3+} species B, could be simulated with the parameters $g_{\perp} = 1.962$ and $g_{\parallel} = 1.944$, as shown in Fig. 6, and is two orders of magnitude more intense than the signal A observed during irradiation. The new signal was stable in the dark indefinitely at 4 K. Re-exposure to broad-band irradiation immediately bleached the signal, and the process of signal growth and disappearance could be repeated many times by turning off and on the broad-band irradiation. The signal also persisted on warming to room temperature in vacuo (when measured again at 4 K), but was immediately and irreversibly removed by exposure to oxygen.

The presence of two different trapped electron sites (the Ti^{3+} EPR signals A and B) was confirmed by irradiating the rutile in vacuo at 4 K with reduced light intensity. Fig. 7 shows the spectrum appearing following broad-band irradiation in vacuo with a reduced lamp power (195 W instead of 450 W). The resulting spectrum shows approximately equal contributions from both Ti^{3+} signals (accurate quantitation is not possible because of the sensitivity of the simulated signals to line widths and line shape functions). The nature of these two trap sites is considered further below.

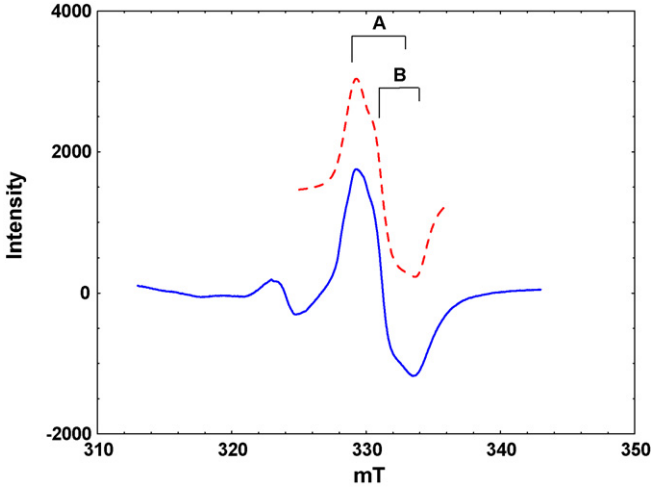

Fig. 7. EPR spectra obtained after irradiation of rutile sample outgassed at room temperature with 195 W of broad-band (320–900 nm) radiation. The dotted trace shows a spectrum simulated as the superposition of the two Ti^{3+} EPR signals A and B described in the text.

A further indication of the presence of at least two different electron trap sites comes from measurements of the kinetics of the appearance of the Ti^{3+} signals when broad-band irradiation is turned off, and their disappearance (bleaching) when the broad-band irradiation is turned on again. These measurements were made by setting the magnetic field to a value corresponding to the intensity maximum in the first derivative traces, and monitoring intensity versus time (the kinetics are therefore predominantly those of signal B, but it is impossible to exclude some contribution from signal A). Fig. 8(a) shows data for the growth of the Ti^{3+} signals when broad-band irradiation at the temperatures indicated was stopped. The curves cannot be fitted to simple exponentials. There appear to be two components to the growth: an initial fast growth which is temperature independent, followed by a slower step which becomes faster at higher temperatures. The corresponding decays in signal intensity when irradiation is resumed (Fig. 8(b)) occur much more rapidly, and show the opposite temperature effect: bleaching occurs more rapidly at the lowest temperature.

The presence of two components in the growth curves is consistent with the spectroscopic evidence for two different Ti^{3+} species, although the signals of species A and B overlap too closely to allow clear separation of their kinetics. Species A is formed first, and may therefore correspond to trap sites deeper within the band-gap than species B.

EPR studies on oxygen deficient single crystals of rutile have identified several different paramagnetic defects [14]. A single interstitial Ti^{3+} defect has an approximately axial g-tensor ($g_1 = 1.978, g_2 = 1.9746, g_3 = 1.9414$). At higher levels of oxygen deficiency, defects comprising pairs of interstitial Ti ions have been identified. The so-called X defect has $S = 1$, and has been described as two interstitial Ti^{3+} ions in close proximity, while the W defect is described as a planar defect involving two titanium ions covalently bonded with a single unpaired electron [14]. The species A and B observed in this work cannot readily be matched directly to the interstitial Ti^{3+} identified in Ref. [14], and the parameters of these signals do not match those of the two dimeric defects in oxygen deficient rutile. We are unable at present to assign with certainty signals A and B to particular Ti^{3+} sites within (or at the surface of) the nanocrystalline rutile. We note however recent theoretical calculations on rutile (1 1 0) surfaces which identify trap sites as Ti ions lying in the first sub-surface layer [15]. Theoretical calculations on n-type anatase by Di Valentin et al. considered four different types of Ti^{3+} in bulk anatase: 6-coordinate Ti^{3+} associated with impurity dopants, 6-coordinate Ti^{3+}–OH, 5-coordinate Ti^{3+} associated with oxide ion vacancies, and 5-coordinate interstitial Ti^{3+} [16]. Since the rutile sample here contains no impurity dopants, and contains no Ti^{3+} sites associated with lattice oxide vacancies prior to irradiation, the two signals we observe are probably due to surface Ti^{3+} and interstitial Ti^{3+}. Signal A, appearing first, is most likely due to interstitial Ti^{3+}, and signal B due to surface sites, but further work is needed to confirm these assignments.

Our proposed explanation for the photo-effects described above is that during broad-band irradiation electrons are excited into the conduction band. Trapping occurs into at least two different trap sites, but trapped electrons are re-excited into the conduction band by the longer wavelength components of the broad-band irradiation, so that a steady-state equilibrium is established between conduction band and trapped electrons (which will be strongly dependent on the photon flux and wavelength range). When the light is turned off, conduction band electrons are trapped, giving

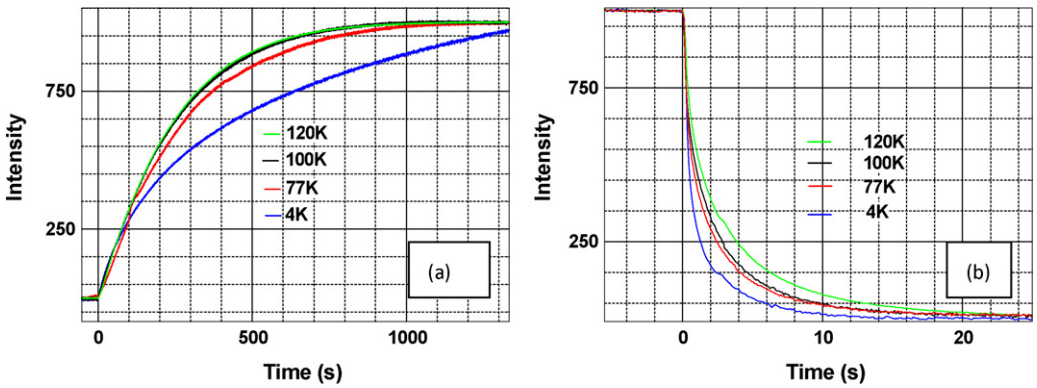

Fig. 8. Time dependence of trapped electron signal following (a) cessation of broad-band irradiation at the temperatures indicated, and (b) following resumption of broad-band irradiation at the temperatures indicated.

the intense EPR signals observed in the dark. When irradiation is resumed, the trapped electrons are re-excited into the conduction band, and the dynamic equilibrium is re-established.

The existence of a steady-state concentration of conduction band electrons during irradiation is well known in anatase from measurements of infrared absorption. Szeczpankiewicz et al. have shown that the free carrier decay lifetime is lengthened as the state of hydration of the surface is decreased (half-life varying between 7.5 and ~100 min) [17]. They suggest a two-step trapping mechanism in which initial slow population of an excited state trap site is followed by a hydration dependent relaxation, which is favoured on more hydrated surfaces. Time resolved microwave conductivity studies, also on anatase, by Savenije et al. [18] showed that the decay of photoconductance (on a microsecond time scale) was thermally activated. The activation barrier for charge trapping was proposed to arise from inter-particle hopping of conduction band electrons, and was estimated to be ~36 meV.

Hole:electron lifetime data are also available for rutile. Conduction band electron lifetimes in anatase and rutile powders have been compared by Colbeau-Justin et al., using time resolved microwave conductivity [19]. Rutile samples showed much faster decays than anatase (10 s of nanoseconds compared with microseconds or longer for anatase at room temperature). The slower recombination rate in anatase was attributed to fast trapping of holes at the anatase surface, thereby inhibiting recombination. Time resolved infrared absorption studies by Yamakata et al. have also shown that recombination is faster in rutile than anatase [20], Schindler and Kunst [21] have discussed the apparent discrepancies between lifetimes measured by time resolved microwave conductivity and laser flash photolysis (<20 ps for colloidal titania dispersions [22]) in terms of laser intensities. They suggest that at high laser intensities direct second order hole–electron recombination dominates, whereas at lower powers decay of conduction band electrons involves trapping.

The trapping processes observed in our EPR experiments appear to be thermally activated. The activation energy is however much less than the 36 meV reported for inter-particle hopping by Savenije et al., since above 100 K there is no further increase in rate. We attribute the opposite effect of temperature on bleaching of the trap sites (increase in rate at lower temperatures) to the competition between trap excitation, trapping, and band-gap excitation into the conduction band. When the rate of trapping is slowed at lower temperatures, emptying of the trap sites occurs more rapidly.

Irradiation with narrow band (400 nm) light produces a much weaker signal of trapped electrons which does not increase when the light is turned off. In this case, we suppose that excitation into the bottom of the conduction band with a lower photon flux produces a lower concentration of conduction band electrons which are quickly trapped i.e. the steady-state equilibrium under irradiation lies in favour of trapped electrons.

A question we cannot answer at this point is: what happens to the positive holes? The generation of intense trapped electron signals following broad-band irradiation which are stable in the dark (in the absence of oxygen) implies that holes have been consumed or trapped in some manner. Only trace amounts of the O^- signal characteristic of trapped holes are detected by EPR, several orders of magnitude less in intensity than the trapped electron signals. We suggest that surface hydroxide ions may play an important role in removing valence band holes. The products of hole trapping are evidently not paramagnetic. Chemistry such as:

$$2OH^- + 2h^+ \rightarrow H_2O_2$$

may be proposed, although we have no evidence at the moment for this reaction. Experiments are now in progress to examine the effects of dehydroxylation of the rutile surface on the electron trapping processes, which may answer the question. An alternative explanation suggested by a referee is that trapped hole (O^-) sites within the interior of the rutile may be EPR invisible if their environment is highly symmetrical (if the degeneracy of the p-orbitals is not sufficiently lifted, then rapid spin-lattice relaxation will broaden the EPR signal beyond detection).

4. Conclusions

The key finding in this work is that in nanocrystalline rutile exposed to broad-band UV–Vis radiation there is a dynamic equilibrium between excitation of electrons from the valence band, trapping of conduction band electrons as Ti^{3+} states within the band-gap, re-excitation from trap states into the conduction band, and recombination. The concentrations of trapped electrons observed by EPR spectroscopy depend on the temperature, photon flux and wavelength. We have also shown that the kinetics of trapping and de-trapping can be followed by low temperature in situ EPR experiments. Results of further studies of the kinetics, the dependence of electron trapping on the state of hydroxylation of the surface, and the wavelength dependence of the de-trapping will be reported elsewhere.

Acknowledgements

Financial support in Aberdeen (R.F.H. and I.R.M.) and St Andrews (W.Z. and X.Z.) was provided by EPSRC. We thank Dr. Terry Egerton for the sample of nanocrystalline rutile.

References

[1] M. Graetzel, R.F. Howe, J. Phys. Chem. 94 (1990) 2566.
[2] T. Berger, M. Sterrer, O. Diwald, E. Knoezinger, D. Panayatov, T.L. Thompson, J.T. Yates, J. Phys. Chem. B 109 (2005) 6061.
[3] T. Berger, M. Sterrer, O. Diwald, E. Knoezinger, ChemPhysChem 6 (2005) 2104.
[4] T. Berger, O. Diwald, E. Knoezinger, M. Sterrer, J.T. Yates, Phys. Chem. Chem. Phys. 8 (2006) 1822.
[5] D.C. Hurum, A.G. Agrios, K.A. Gray, J. Phys. Chem. B 107 (2003) 4545.
[6] D.C. Hurum, A.G. Agrios, S.E. Crist, K.A. Gray, T. Rajh, M.C. Thurnauer, J. Electron. Spec. Rel. Phen. 150 (2006) 155.
[7] K. Komaguchi, H. Nakano, A. Araki, Y. Harima, Chem. Phys. Lett. 428 (2006) 338.
[8] C.P. Kumar, N.O. Gopal, T.C. Wang, M.S. Wong, S.C. Ke, J. Phys. Chem. B 110 (2006) 5223.
[9] S. Yang, L.E. Haliburton, A. Manivannan, P.H. Bunton, D.B. Baker, M. Kiemm, S. Horn, A. Fujishima, Appl. Phys. Lett. 94 (2009) 162114.
[10] K. Komaguchi, T. Maruoka, H. Nakano, I. Imae, Y. Ooyama, Y. Harima, J. Phys. Chem. C 113 (2009) 1160–1163.
[11] R. Scotti, I.R. Bellobono, C. Canevali, C. Cannas, M. Catti, M. D'Arienzo, A. Musinu, S. Polizzi, M. Sommariva, A. Testino, F. Morazzoni, Chem. Mater 20 (2008) 4051.
[12] N. Serpone, D. Lawless, R. Khairutdinov, J. Phys. Chem. 99 (1995) 16646.
[13] M.M. Mikhailov, Inorg. Mater. 40 (2004) 1054.
[14] M. Aono, R.R. Hasiguti, Phys. Rev. B 48 (1993) 12406.
[15] N.A. Deskins, R. Rosseau, M. Dupuis, J. Phys. Chem. C 113 (2009) 14583.
[16] C. Di Valentin, G. Pacchioni, A. Selloni, J. Phys. Chem. C 113 (2009) 20543.
[17] S.H. Szczepankiewicz, J.A. Moss, M.R. Hoffmann, J. Phys. Chem. B 109 (2005) 2922.
[18] T.J. Savenije, A. Huijser, M.J.W. Vermeulen, R. Katoh, Chem. Phys. Lett. 461 (2008) 93.
[19] C. Colbeau-Justin, M. Kunst, D. Huguenin, J. Mater. Sci. 38 (2003) 2429.
[20] A. Yamakata, T. Ishibashi, H. Onishi, Chem. Phys. 339 (2007) 133.
[21] K.M. Schindler, M. Kunst, J. Phys. Chem. 94 (1990) 8222.
[22] G. Rothenberger, J. Moser, M. Gratzel, N. Serpone, D. Sharma, J. Am. Chem. Soc. 107 (1985) 8054.